

Characterisation of Syngas Laminar Diffusion Flame with an Effect of its Varying Composition

Tananop Piemsinlapakunchon, and Manosh C. Paul

Abstract—Syngas (H_2/CO) and syngas- CH_4 co-flow laminar diffusion flames are studied with a particular aim of investigating the effect of various H_2 , CO , and CH_4 contents on the flame characteristics (e.g. flame structure, temperature, and heat release) and also on the emission of CO_2 and NO_x . Finite rate chemistry algorithm, multi-component diffusion, thermal diffusion and radiation model are selected for solving the continuity, momentum, energy, and specie transport equations. Composition of fuel is varied to project the effect of content of each species containing in fuel composition. Heat release from the syngas flame at various $H_2:CO$ ratio is also compared.

Index - Laminar Diffusion Flames; Syngas Combustion; Numerical modelling; Flames characteristics

I. INTRODUCTION

Syngas, mixture of fuel gases containing primarily hydrogen (H_2) and carbon monoxide (CO), is one of the interesting options among various types of clean and sustainable energy. Multiple options in the production processes and feedstocks are the key factors attracting research and development on this fuel. As various processes and feedstocks can be utilized, composition of produced syngas is varied.

Mixtures of H_2 , CO , CO_2 , N_2 , H_2O and CH_4 at different volume fraction are resulted as shown in recent literatures [1-5]. In order to combust this fuel effectively, improve production process and design of a suitable combustion system which can extract the highest possible performance from the fuel combustion, an in-depth analysis of these fuel compositions is necessary.

II. MODEL FORMULATION

The selected co-flow burner is the same one presented in [6] where it was used for studying a H_2/N_2 laminar diffusion flame. Appearance of this burner is presented in Fig 1. The fuel inlet is a round tube located at the center with an inner diameter of 9 mm. This inlet is surrounded by a 95 mm inner diameter co-flow air inlet. The thickness of the fuel tube is defined as 1 mm and the position of the fuel exit is 8

mm higher than the co-flow air. Both fuel and air are injected vertically in the opposite direction to the gravitational force.

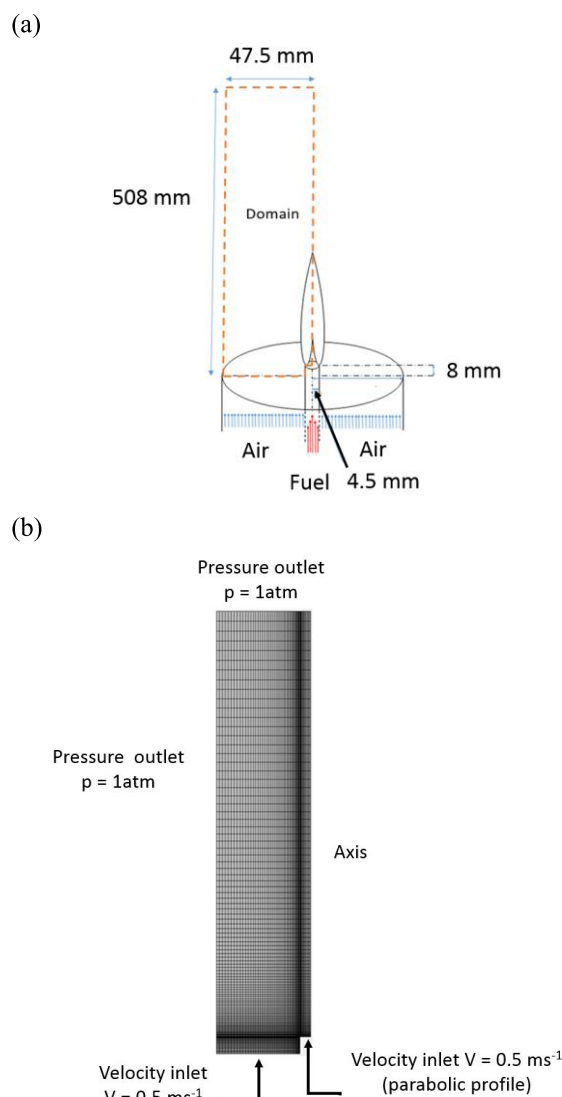


Fig 1 (a) burner geometry and area of interest (b) generated mesh and boundary condition

To model this burner, an axisymmetric domain is generated based on the geometry of the burner as shown in Fig 1. Area of interest is the section above the fuel and air inlet. The width of the top plane is 4.75 cm accounted from the center line of the fuel tube to the outer line of the co-flow air tube horizontally. The width of the bottom plane is 4.2 cm and is between the outer of co-flow air and the outer of fuel tube. Distance between the top and bottom planes is 50.8 cm. Fuel inlet width is 0.45 cm from the center line and

is 0.8 cm above the air inlet. This setup takes into account the effect of fuel tube on the flow of co-flow air due to different level between the co-flow air inlet and fuel inlet (8 mm).

In terms of boundary condition, the top and left planes are defined as a pressure boundary. Pressure and temperature at these boundaries are 101325 Pa and 298 K respectively. Right plane is set as axis. Fuel and co-flow air inlet are velocity inlet boundary. Profile of the fuel stream is parabolic while one of the co-flows is bulk profile. Both streams are injected at an equal average velocity of 50 cm/s and temperature of 298 K. Vertical plane connected between the fuel and co-flow air inlets is a wall boundary with temperature of 298 K.

Non-uniform mesh is generated through a hyperbolic function. The smallest cell size is 2×10^{-4} m and is located at the outer of fuel tube and the same level as fuel exit. The number of grid points in the vertical direction is 500 and 24 from the smallest cell position to the top plane and co-flow inlet respectively. In the horizontal direction, 50 and 16 are used from the smallest cell location to the left outlet plane and axis. A total of 17,950 cells is produced based on this setup which is illustrated in Fig. 1(b).

III. GOVERNING EQUATIONS

The governing equations are presented as follows:

Continuity equation

$$\frac{\partial \rho}{\partial t} + (\rho \vec{V}) = 0 \quad (1)$$

Momentum equation

$$\frac{\partial(\rho \vec{V})}{\partial t} + \nabla \cdot (\rho \vec{V} \vec{V}) = -\nabla p + \nabla \cdot \vec{\tau} + \rho \vec{g} \quad (2)$$

Where

$$\vec{\tau} = \mu[\nabla \vec{V} + \vec{V}^T - \frac{2}{3} \nabla \vec{V} I]$$

Species transport equation

$$\frac{\partial(\rho \vec{V})}{\partial t} + \nabla \cdot (\rho \vec{V} Y_i) = -\vec{V} \cdot \vec{J}_i + R_i + S_i \quad (3)$$

Energy equation

$$\nabla \cdot (\vec{V}(\rho E + p)) = \nabla \cdot (k \nabla T - \sum_j h_j \vec{J}_j + (\vec{\tau} \cdot \vec{V})) + S_h \quad (4)$$

Where

$$E = h - \frac{p}{\rho} + \frac{v^2}{2} \quad \text{and} \quad h = \sum_j Y_j h_j$$

Multi component diffusion is considered as well as thermal diffusion as shown in (5). The previous one is computed through Maxwell-Stefan equation while the later one is calculated by Warnatz model. Details of them can be found in [7] and [8].

$$\vec{J}_i = -\rho \left(\sum_{j=1}^N D_{i,j} \nabla Y_j \right) - \rho \frac{D_{T,i}}{T} \nabla T \quad (5)$$

Dynamic viscosity and thermal conductivity are defined by Chapman-Enskog method and kinetic theory respectively. These are illustrated in (6) and (7).

$$\mu_i = 2.6693 \times 10^{-6} \frac{\sqrt{M_i T}}{\sigma_i^2 \Omega(T^*)} \quad (6)$$

$$\lambda_i = \frac{\mu_i}{M_i} (f_{tran} C_{v,tran} + f_{rot} C_{v,rot} + f_{vib} C_{v,vib}) \quad (7)$$

Participating media radiation model is selected for computing radiation. Discrete Ordinates Method (DOM) is utilized for solving the radiation transport equation [7]. Absorption coefficient is calculated through weight sum of grey gas model (WSGG). Total absorptivity of several grey gases is approximated as shown in (8). The medium is assumed to consist of different fractions of grey gases with different absorption coefficients. CO₂ and H₂O are assumed to dominate cloud emission and absorption among the combustion gas products.

$$\alpha \approx \sum_{k=0}^K a_k (1 - e^{-K_k S}) \quad (8)$$

The medium is assumed to be optically thin. Optical path length (S) is defined as:

$$S = 3.6 \frac{\text{Volume of the domain}}{\text{surface area of domain}} \quad (9)$$

GRI3 reaction mechanism containing 53 species and 325 reactions is selected and the governing equations are solved by using STAR-CCM CFD software.

IV. VALIDATION OF MODELLING RESULT

All the H₂/N₂ flames presented in [6] are simulated by the generated model, and the experimental and numerical results of [8] are initially compared with the numerical results of our model. Well agreement is obtained from the comparison on species (H₂, N₂, O₂, and H₂O) and temperature profiles. This confirms the reliability and accuracy of the GRI3 chemistry mechanisms and newly generated CFD model, thus the simulations of other flames having different fuel compositions are proceed with full confidence.

V. SIMULATION SETUP

To investigate the effect of H₂, CO, and CH₄ on the flame characteristics, flames having various volume fraction of these species are simulated. Details of these flames are presented in Table 1. For syngas flame, volume fraction of H₂ and CO are varied between 25 and 75 % whereas volume percentage of CH₄ is set as 10 – 20% in the syngas-CH₄ flame. Pure H₂ and pure CH₄ are formulated for assessing the performance of syngas and syngas-CH₄ flames. Average velocity of fuel and co-flow air are set equally as 0.5 ms⁻¹ for all the flames. This flow condition will maintain a volume flow rate of injected fuel of 31.8 cm³s⁻¹ respectively.

TABLE 1 SIMULATED FLAMES

Flame	H ₂ (%)	CO (%)	CH ₄ (%)	ρ (kg-m ⁻³)
A	100	0	0	0.0824
B	75	25	0	0.3480
C	50	50	0	0.6139
D	25	75	0	0.8790
E	45	45	10	0.6224
F	40	40	20	0.6182
G	0	0	100	0.6560

VI. RESULTS AND DISCUSSION

A. Flame structure, temperature and heat release

Temperature contour of Flames B, C, D, E, and F are shown in Fig 2a along with a chart representing the maximum flame temperature and flame length in Fig 2b. As seen, the flame temperature strongly depends on the fuel composition and the content of H₂ in fuel has a significant role on temperature. E.g. Flames having a higher volume fraction of H₂ has a higher flame temperature. The highest maximum temperature is obtained from Flame A (100% H₂) 2319 K followed by flame B (75% H₂) 2227 K. In turns, the lowest maximum temperature is found on Flame G (0% H₂) followed by Flame D (25% H₂). This finding is similar to what reported in [4] and a higher flame temperature was obtained from an enrich H₂ syngas flame.

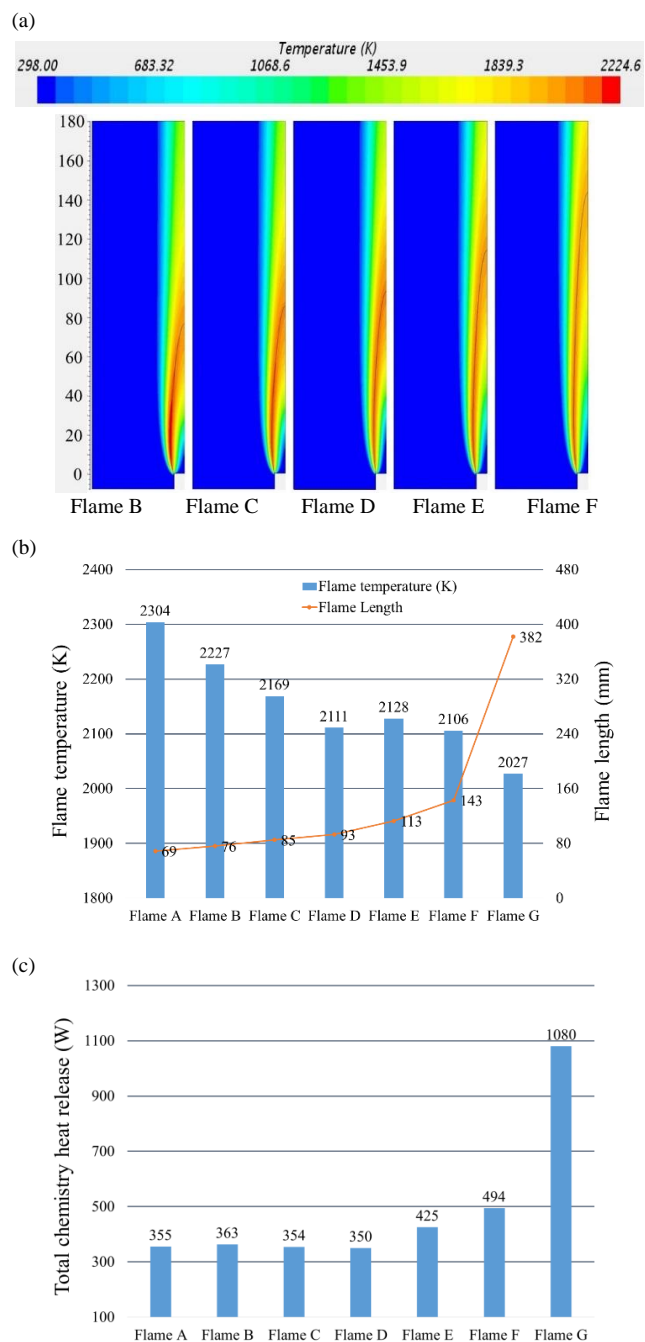


Fig 2 (a): temperature contour of syngas and syngas-CH₄ flames; (b): maximum temperature and flame length; (c) total chemistry heat release

Analyzing the flame structure, the position of maximum flame temperature of every flame is located slightly above and close to the outer of fuel exit. Burner configuration and flow condition are the causes of this appearance. Flame width is slightly different and Flames having a higher H₂ content is thicker than the lower content ones. This supports the result of [6]. But, species containing carbon content play an important role on the flame length. Syngas and syngas-CH₄ flames containing higher volume fraction of CO and CH₄ have longer flame length. Stronger effect is found from CH₄ and adding 10% of this specie increases the flame length approximately 20 mm. Supporting this finding, Flame G which is a pure CH₄ flame has the longest flame among all the simulated flames followed by Flame F which contains 20% of CH₄. Both the flame length and flame temperature are strongly dependent on the fuel composition.

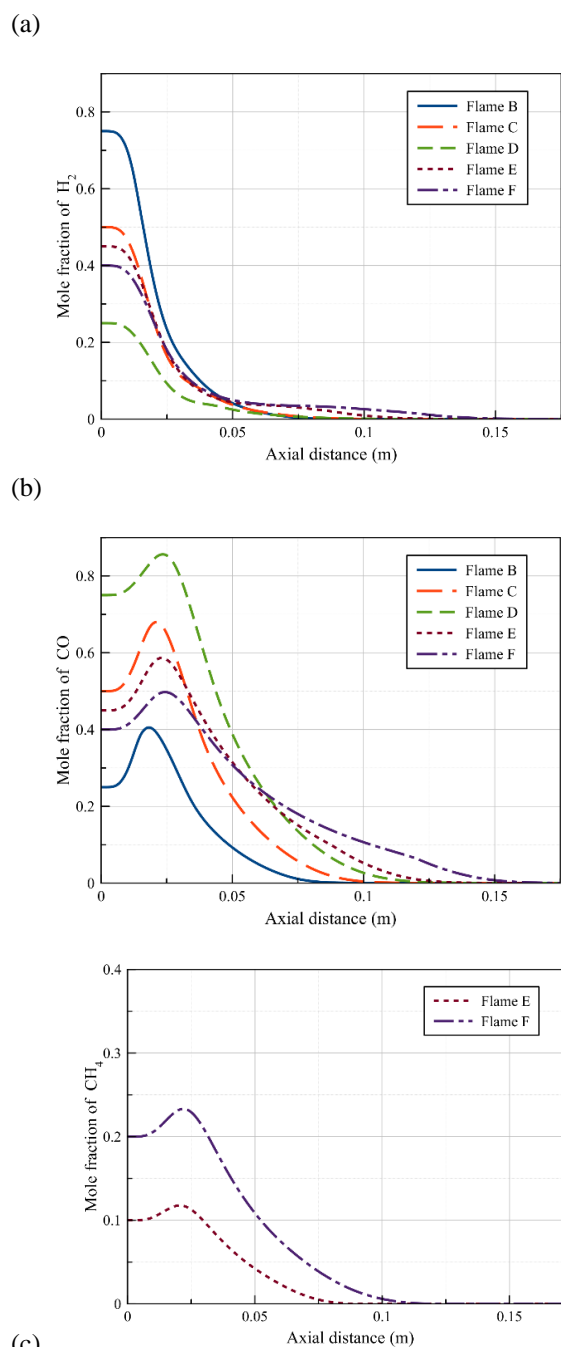


Fig 3 Species distribution of (a) H₂, (b) CO, and (c) CH₄

The total chemistry heat release from all the Flame cases is presented in Fig 2(c). The highest chemistry heat release is found on Flame G (1080 W) followed by Flame F (494 W). Chemistry heat release of the syngas flame can be considered as comparable. Though their flame dimension and fuel composition are different, all syngas flames release similar amount of heat between 354 and 363 W. Longer flame length compensates with lower flame temperature. This thus causes the syngas flames having lower temperature (with higher content of CO) providing similar amount of heat.

Moreover, this amount is similar to the chemistry heat release of pure H₂ flame (355 W). As longer flame can also provide higher heat release, Flame E, F, and G containing higher amount of CH₄ with having significant longer flame than syngas flame can provide significant higher heat release compared to syngas and pure H₂ flame. Addition of 10 % of CH₄ to syngas increases approximately 70 W of chemistry heat release. This amount is about 20 % escalation.

B. Species distribution

Axial profile of H₂, CO and CH₄ of Flames B, C, D, E, and F are shown in Fig. 3(a-c). Mole fraction of H₂ is significantly reduced along the axis and approaches zero at location under the flame front. This high reduction gradient at the distance close to the fuel exit refers to a fast burning rate of H₂. Shorter flame length with a having higher H₂ content is the result of this phenomenon.

Profile of CO however increases significantly to the peak value, which is approximately 0.1-0.18 of the mole fraction above the CO volume fraction in fuel, then reduces meaningfully to reach zero mole fraction at location slightly under the flame front. Lower reduction gradient is resulted comparing to the profile of H₂ which represents a slower burning rate of CO compared to H₂. It suggests a longer axial distance is required in order to fully consume the CO content. This leads to the longer flame length of syngas having a higher volume fraction of CO.

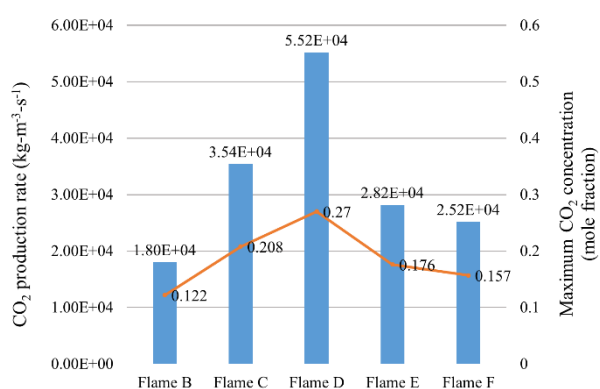


Fig 4 Production rate and maximum concentration of CO₂

Profile of CH₄ is similar to CO as both are carbon fuel species. Mole fraction increases from the injected value to a peak value which is approximately 0.12 and 0.24 in Flame E and F respectively. Slow burning rate of CH₄ can also be seen after the peak position. Consumption of 20% volume fraction of CH₄ requires a similar distance of 75% of CO. This results in a strong effect of CH₄ content in fuel

composition on the flame dimension. The other effect of CH₄ is on the extension of distance required for fully consumption of CO. Analysis of the CO and CH₄ profiles of Flames C, E, and F projects the change of consumption rate of CO when content of CH₄ is added.

It is shown in Fig. 4 that the CO₂ formation, production rate and maximum concentration of CO₂ depend strongly on the CO content in fuel. Higher volume fraction of CO increases the production rate of CO₂ and produces the higher peak concentration of CO₂. The highest maximum rate and peak concentration is computed from Flame D which contains 75% of CO. The second highest rate is resulted from Flame C which contains 50% CO in the fuel composition. Direct proportion can be considered for a relation between the volume fraction of CO and CO₂ formation.

VII. CONCLUSION

Effect of fuel composition on the characteristics and emission from the co-flow laminar diffusion flames of syngas, syngas-CH₄, pure H₂ and pure methane are studied. Finite rate chemistry model along with multi-component diffusion, thermal diffusion, and radiation model are selected. Following key conclusions can be drawn from the findings:

- (i) Content of H₂ has a significant role on the flame temperature and dimension. Flames having a higher volume fraction of H₂ have a higher flame temperature with a wider, and shorter dimension. Effect on the dimension is found to be the faster burning property of H₂ comparing to that of CO and CH₄.
- (ii) Lower burning rate of CO than H₂ leads to the longer flame dimension of syngas with a higher volume fraction of CO. This effect provides similar total chemistry heat release of enrich-CO flame to enrich-H₂ which has a higher flame temperature. Longer flame dimension results in more area of grid generating heat release. This finally increases the total heat release.

(iii) CH₄ is found to have the slowest burning rate along the axis. This property causes flame having higher content of CH₄ thus taking longer distance to be fully consumed. Significantly long flame length is the result. Similar to CO, the longer flame length compensates the lower flame temperature of CH₄. This causes the higher CH₄ content flame having a higher heat release and heat flux. Moreover, lower flame temperature property of CH₄ can reduce emission amount from syngas as H₂ and CO content are reduced from fuel composition.

NOMENCLATURE

Uppercase letters

- C_v Contribution to the molar specific heat of each specie
- $D_{t,i}$ Thermal diffusion coefficient
- $D_{i,j}$ Molecular diffusivity of multi component gases
- $F_{k,j}$ Diffusive flux component
- I Unit tensor
- J Diffusive flux
- K_k Absorption coefficient of each grey gases
- K Total number of grey gases
- M Molecular weight

S Optical path length
 S_h Heat due to chemical reaction and radiation
 T Temperature
 T^* Reduced temperature
 V Velocity
 Y Mass fraction

Greek letters

ρ Fluid density
 σ Collision diameter
 $\vec{\tau}$ Viscous stress tensor
 μ Molecular viscosity
 Ω Collision integral
 λ Thermal conductivity

Lowercase letters

a_k Weight factor
 g Gravitational acceleration
 h Specific enthalpy
 k Thermal conductivity coefficient
 p Pressure
 t Time
 v Velocity

Subscripts

i component i
 j Specie j
 k Specie k
 $tran$ Translation
 rot Rotation
 vib Vibration
 avg Average

ACKNOWLEDGEMENT

The lead author would like to express his gratitude to Royal Thai Navy for supporting his Phd research at University of Glasgow.

REFERENCES

- [1] J. Park, D. S. Bae, M. S. Cha, J. H. Yun, S. I. Keel, H. Chang Cho, T. K. Kim and J. S. Ha, "Flame characteristics in H₂/CO synthetic gas diffusion flames diluted with CO₂: Effects of radiative heat loss and mixture composition," International Journal of Hydrogen Energy, vol. 33, no. 23, pp. 7256-7264, 2008.
- [2] J. Park, O. B. Kwon, J. H. Yun, S. I. Keel, H. Chang Cho and S. Kim, "Preferential diffusion effects on flame characteristics in H₂/CO syngas diffusion flames diluted with CO₂," International Journal of Hydrogen Energy, vol. 33, no. 23, pp. 7286-7294, 2008.
- [3] S. Hsin-Yi, H. Jou-Rong and L. Yu-Heng, "Computed flammability limits of opposed-jet H₂/CO syngas diffusion flames," International Journal of Hydrogen Energy, vol. 39, no. 7, pp. 3459-3468, 2014.
- [4] A. Cuoci, A. Frassoldati, G. Buzzi Ferraris, T. Faravelli and E. Ranzi, "The ignition, combustion and flame structure of carbon monoxide/hydrogen mixtures. Note 2: Fluid dynamics and kinetic aspects of syngas combustion," International Journal of Hydrogen Energy, vol. 32, no. 15, pp. 3486-3500, 2007.
- [5] K. Ranga Dinesh, X. Jiang, M. Kirkpatrick and W. Malalasekera, "Combustion characteristics of H₂/N₂ and H₂/CO syngas nonpremixed flames," International Journal of Hydrogen Energy, vol. 37, no. 21, pp. 16186-16200, 2012.
- [6] V. V. Toro, A. V. Mokhov, H. B. Levinsky and M. D. Smooke, "Combined experimental and computational study of laminar, axisymmetric hydrogen-air diffusion flames," Proceedings of the Combustion Institute, vol. 30, no. 1, pp. 485-492, 2005.
- [7] cd-adapco, "STAR CCM+ version 11 User guide," Cd-adapco, 2016. [Online]. Available: <https://stevedocs.cd-adapco.com/>
- [8] J. Warnatz, U. Maas and R. W. Dibble, Combustion: Physical and Chemical Fundamentals, Modeling and Simulation, Experiments, Pollutant Formation, Berlin, Germany: Springer, 2006.